Published in final edited form as:
Cancer Gene Ther. 2013 November ; 20(11): 630–637. doi:10.1038/cgt.2013.58.

Inhibition of Rho associated coiled-coil forming kinase increases efficacy of measles virus infection *in vitro* and *in vivo*

Mateusz Opyrchal, MD, PhD[1,2], **Cory Allen**[2], **Pavlos Msaouel, MD**[3], **Ianko Iankov, MD, PhD**[2], and **Evanthia Galanis, MD**[1,2]

[1]Division of Medical Oncology, Mayo Clinic, 200 First Street SW, Rochester, MN

[2]Department of Molecular Medicine, Mayo Clinic, 200 First Street SW, Rochester, MN

[3]Albert Einstein College of Medicine, Jacobi Medical Center, Department of Internal Medicine, Bronx, NY

Abstract

RhoA and its downstream effector, Rho associated coiled-coil forming kinase (ROCK) are known regulators of formation of actin cytoskeleton in cells. Actin cytoskeleton is involved in paramyxovirus infection. We examined the effect of ROCK inhibition on MV cytopathic effect and replication. Treatment with specific ROCK inhibitor, Y27632, significantly increased syncytia size in 2 cell lines following MV infection, associated with cytoskeleton disruption as demonstrated by actin staining. 3 different cell lines infected with MV while concurrently treated with Y27632 showed increased cytopathic effect following viral infection as assessed by trypan blue exclusion assays. In these cells, there was a significant increase in viral proliferation after day two by at least one log or more as tested in one step viral growth curves. Increased viral replication was also observed in athymic nude mice bearing MDA-MB-231 xenografts following combination treatment with MV and Y27632. Inhibition of ROCK kinase by Y27632 enhanced oncolytic effect of MV on prostate, breast and glioblastoma cancer cells. Increased cell killing was correlated with higher viral titers and larger syncytia. The Y27632 effect on cellular cytoskeleton likely accounts for the larger syncytia size.

Introduction

Virotherapy is being studied as an attractive new option for treating various malignancies. One of the major hurdles of this treatment strategy is the innate immunity. Measles virus (MV) is a negative strand RNA virus and attenuated strains deriving from the Edmonton vaccine lineage have antitumor activity against multiple cancer types *in vitro* and *in vivo*. MV vaccine strains enter cells primary through the CD46 receptor as well as the recently identified receptor Nectin-4[1–3], as opposed to the SLAM receptor predominantly used by wild type MV. Infected cells fuse with neighboring cells with formation of multinucleated syncytia[4–7], which can result in significant bystander effect. Cytoskeleton has been shown to be an important component in paramyxoviruses replication.[8] Although the role of cellular cytoskeleton in MV infection has not been completely elucidated, actin is thought to play a role in virion maturation and release[9–12] as well as membrane fusion[13].

Corresponding Author: Evanthia Galanis, M.D., Mayo Clinic, 200 First Street SW, Rochester, MN 55905, Phone: (507) 284-3902, Fax: (507) 284-1803, galanis.evanthia@mayo.edu.

The authors report no conflicts of interest.

RhoA belongs to family of GTPases and it plays a crucial role in multiple cellular processes among them cytoskeleton regulation, cell adhesion and migration.[14,15] Rho associated coiled-coil forming kinases (ROCK) and mDia are downstream effectors of Rho.[14,16–19] ROCK is a serine/threonine kinase and has been shown to phosphorylate the myosin-binding subunit of myosin phosphatase as well as myosin light chain. These actions result in increased myosin phosphorylation/cross-linking of actin cytoskeleton and increased contractility.[20,21] Rho/ROCK has been implicated in cell migration through its effects on integrins and cell adhesion.[22,23] RhoA has also been shown to contribute to malignant transformation.[24] Another Rho isoform, RhoC, has been associated with increased metastatic potential in human cancer tissue.[25,26]

We hypothesized that since regulation of cytoskeleton plays an important role in MV replication, inhibition of ROCK can lead to enhancement of efficacy of MV virotherapy. We showed that by inhibiting ROCK we increase cell fusogenicity after infection with MV, with increased cell killing and generation of higher virus titers in vitro. We also confirmed increased viral replication *in vivo* in mice treated with the MV/ROCK inhibitor combination.

Results

Treatment with Y27632 causes increased measles virus induced syncytia *in vitro*

Initially we examined the ability of the Y27632 to inhibit cellular proliferation. Concentrations with minimal effect on cellular proliferations were used in subsequent experiments in order to evaluate its effect on MV replication (data not shown). Next we determined the optimal sequence of MV infection/Y27632 treatment. We tested different sequences of Y27632 treatments ranging from 24 hours prior to 24 hours post infection and determined that the best effect was observed when cells were treated with Y27632 up to six hours post infection. Increased size of MV induced syncytia was observed across different tumor types with representative results in MDA-MB-231 breast cancer cells shown in figure 1A. We used NIH ImageJ software to quantify the size of the syncytia in MDA-MB-231 and DU-145 cell lines. Treatment with Y27632 significantly increased the syncytia size of MV infected cells in both MDA-MB-231 and DU-145 cell lines (Figure 1B and C).

Treatment with Y27632 results in disruption of the actin cytoskeleton

It has been previously shown that inhibition of ROCK disrupts actin cytoskeleton therefore we wanted to investigate if Y27632 at concentrations, which increase syncytia size, has an effect on the actin cytoskeleton. As shown in Figure 2 treatment with Y27632 concentrations that affected syncytia formation over a period ranging from 24 to 48 hours had a profound effect on the actin cytoskeleton and induced distinctive phenotype in MDA-MB-231 and DU-145 cells. In cells treated with Y27632 there is a distinct disruption of the actin cytoskeleton and increase in staining for actin filaments.

Treatment with Y27632 causes increased measles virus induced cytopathic effect *in vitro*

Next, we explored the question of whether increase in syncytia size is associated with increased cell death following treatment with MV in combination with Y27632. We explored this question in MDA-MB-231 (breast cancer) and U251 (glioma) cell lines. Cells were infected with MV at a MOI of 0.1 with concentrations of Y27632 which were previously determined to have minimal effect on cell proliferation. In both cell lines the combination therapy was superior to either treatment alone in its oncolytic effect as determined through trypan blue exclusion assays (Figure 3A). This effect was dependent on concentration of Y27632 as shown in Figure 3B. On day 6 following infection, 50% of cells were viable versus only 43% cells being viable ($p=0.0158$) following combination of MV and 75 μM Y27632 and 23% with 150 μM of Y27632 ($P=0.0017$ when compared to 75 μM

treated cells). Y27632 single agent treatment had minimal impact on cell proliferation at the same concentrations.

Treatment with Y27632 leads to increased MV replication *in vitro*

In order to examine the effect of Y27632 on MV replication, we determined viral replication in three cell lines (MDA-MB-231, U251, DU-145) by one step viral growth curves. As seen in figure 4A there was a significant increase in the amount of virus particles recovered in all three cell lines following combination treatment. As figure 4B shows, the impact of Y27632 on viral replication was dependent on the concentration of the drug; increasing concentrations of Y27632 resulted in significant increases in MV. To confirm these findings we examined levels of viral N protein expression in the infected cells. As figure 5 demonstrates, there is an increase in nucleocapsid (N) protein in cells treated with Y27632 as compared to cells infected with MV alone. In order to further examine the effect of Y27632 treatment on viral gene expression, an MV strain engineered to express the human lambda light chain was used (MV-Lambda) (Figure 6A), with levels of lambda light chain serving as a correlate to viral replication. MDA-MB-231 cells treated with Y27632 after infection with MV-Lambda had a statistically significant increase in lambda production as compared to cells infected with virus alone (Figure 6B) 48 hours ($p=0.0157$) and 72 hours ($p=0.0002$) after infection. These experiments demonstrate that treatment with Y27632 leads to increased MV replication *in vitro* in breast, glioma and prostate cancer cell lines.

We also asked the question if the ability to form syncytia is necessary for the observed effect of Y27632 on viral replication. MDA-MB-231 cells were infected with MV-Lambda and then treated with fusion inhibitory peptide (FIP) in addition to Y27632. FIP abrogated the ability of the MV to form syncytia and decreased viral replication. As shown in figure 7 there was significant decrease in lambda in the supernatant of cells treated with FIP/MV-lambda combination as compared to control cells infected with MV-Lambda alone. Addition of Y27632 did not increase the production of lambda (figure 7). Therefore, syncytia formation is necessary for the Y27632 to enhance MV replication.

Y27632 increases viral replication *in vivo*

The ability of Y27632 to increase viral replication was also tested *in vivo* in MDA-MB-231 cell flank mouse tumor model. The flank tumors were injected with one dose of MV-Lambda ($2.0*10^6$ $TCID_{50}$). The mice were treated with PBS or Y27632 dissolved in PBS intraperitoneally at a dose of 10 mg/kg twice daily for 5 days. On day 5 blood was obtained from the mice and serum was tested for the levels of human lambda light chain. The level of human lambda was elevated in mice treated with MV-Lambda indicating viral replication. Statistically significant increase in human lambda levels in mice treated with Y27632 ($p=0.0462$) was detected. There was no clinically observed toxicity in association with Y27632 therapy.

Discussion

Virotherapy is a novel and highly promising new treatment option for patients with variety of malignancies. The MV vaccine strains represent a potent oncolytic platform with activity against a variety of solid as well as hematologic malignancies in vitro and in vivo including glioblastoma[27–33], breast[34,35], multiple myeloma[36], medulloblastoma[37,38], prostate[39,40] and hepatocellular[41] cancers. The pre-clinical results have led to clinical testing of the MV in patients with ovarian cancer[42], multiple myeloma, mesothelioma, glioblastoma and head and neck cancers. Promising early clinical activity was observed in ovarian cancer patients[43] while clinical data in other tumor types is maturing. Further increasing the efficacy of

measles virotherapy by exploring combination strategies is the translational question that the second generation trials will address.

Paramyxoviridae have been shown to interact with cellular actin.[44–46] Actin alterations have also been associated with changing of fusogenicity of cells during viral infection.[13] Rho family GTPases are involved in multiple cellular function one of which involves actin cytoskeleton regulation.[14,15] Rac1 has been found to play a role in modulating actin cytoskeleton during viral infection.[47] Therefore, we explored a role of ROCK, downstream effector of Rho GTPases, in actin cytoskeleton modulation and fusogenicity during MV infection.

Y27632 is a specific ROCK inhibitor[48]. Treatment of cancer cells with Y27632 leads to decreased cell mobility and metastatic potential[16,49–52], prevention of malignant transformation[53] as well as increased apoptosis[54]. Y27632 treatment leads to increased expression of integrins and subsequent overexpression of adhesion molecules. Treatment with Y27632 following measles infection increases syncytia size, which results in higher viral titers and antitumor effect. The mechanism of increased fusogenicity is likely related to the effect of Y27632 on the actin cytoskeleton in cells treated with MV/Y27632 combination; of note, the cytoskeleton changes induced by Y27632, not only did not adversely affect MV replication but actually increased it in a syncytia dependent manner.

Rho/ROCK pathway is currently under increasing scrutiny, although its importance in human cancer is still under investigation. Several mutations of Rho proteins have been identified[55] and they have been found to be overexpressed in several human cancers[25,56]. There have been increasing development and pre-clinical data on effectiveness of ROCK inhibitors[16] in breast[57], melanoma[58], hepatocellular[59] cancers. Combining this new class of drugs with MV may lead to a synergistic anti-tumor effect.

In summary we showed that ROCK inhibition leads to enhanced syncytia formation, increased cytopathic effect as well as increased viral replication of MV. Enhanced MV replication with ROCK inhibitor co-treatment was also seen in a breast cancer animal model. These results contribute to better understanding of the importance of the Rho/ROCK pathway in measles oncolytic virotherapy and encourage the investigation of future translational application of combining MV strains with ROCK inhibitors or other cytoskeleton modifying agents.

Material and Methods

Viruses

Attenuated MV Edmonston vaccine strain was used as a platform for generation of recombinant MV constructs. Recombinant MVs encoding the full lambda immunoglobulin chain (MV-lambda)[60] and the enhanced green fluorescent marker protein (MV-GFP)[61] were constructed as previously described. The viruses were propagated in Vero cells and titrated as previously described[39,62].

Cell lines

VERO (African green monkey) cell line and human cancer cell lines DU-145 (prostate cancer), U251 (glioma) and MDA-MB-231 (breast cancer) were purchased from American Type Culture Collection (ATCC, Manassas, VA). All cell lines were grown at 37 °C in media recommended by ATCC in a humidified atmosphere of 5% CO_2. All media contained 100 U/ml penicillin-streptomycin and were supplemented with 10% heat-inactivated fetal bovine serum.

Assessment of MV replication in cancer cell lines

DU-145, U251 and MDA-MB-231 cells were plated in six-well plates at a density of 5×10^5 cells/well. Twenty-four hours after seeding, the cells were infected with MV-GFP at MOI of 0.1 in 0.5 – 1.0 ml of Opti-MEM for 2 to 4 hours at 37 °C. At the end of the incubation period, the virus was removed and the cells were treated with Y27632 (Sigma-Aldrich, St. Louis, MO) dissolved in DMSO at stock solution of 100 mM, at the specified concentrations, equivalent amount of DMSO was added to control wells in their standard medium. Cells were harvested at specified time points from (different wells per time point) and MV-GFP was released by two cycles of freezing/thawing. The viral titer at each well was determined by 50% end-point dilution assay ($TCID_{50}$) on Vero cells in a 96-well plate[34]. Results are presented as the means of three independent experiments ± SEM.

Assessment of syncytia size

Cancer cells (MDA-MB-231 and DU-145) were infected with MV-GFP at MOI 0.01 and then treated with Y27632 as described above. Cells were fixed with formaldehyde and crystal violet stained at 72 hours post MV-GFP infection. Photographs were taken in 4 corners and center of two wells per time point. Quantitation of the syncytial surface per plate was performed using NIH Image J software (version 1.46) and results were expressed as number of pixels per syncytia.[63]

Assessment of the cytopathic effect *in vitro*

U251 and MDA-MB-231 cells were plated in six-well plates at a density of 5×10^5 cells/well. Twenty-four hours after seeding, the cells were infected with MV-GFP at a MOI of 0.1 in 0.5 – 1.0 ml of Opti-MEM for 2 hours at 37 °C. At the end of the incubation period, the virus was removed and the cells were treated with Y27632 at 75–150 μM; equivalent amount of DMSO was added to control wells in their standard medium. The same number of uninfected cells was used as controls. The cells were harvested at days 4, 7, 10 (MDA-MB-231 cells) and days 4, 6, 8 (U251 cells) from two different wells per time point and viable cells were counted on hemocytometer. Viable cells were identified using trypan blue staining. The percentage of surviving cells was calculated by dividing the number of viable cells in experimental wells by the number of viable cells in the uninfected wells corresponding to the same time.

Actin Staining

Tumor cells were plated on tissue culture microscope slides. Y27632 was added at specified time points and all cells were incubated for 48 hours. Cells were then stained using Invitrogen Alexa Fluor® 488 Phalloidin Conjugate (Invitrogen, Carlsbad, CA) as per the manufacturer's instructions. Briefly, cells were fixed in 3.7% formaldehyde solution and then permeabilized with 0.1% Triton X-100 solution. Afterwards they were incubated with Alexa Fluor® 488 Phalloidin Conjugate (Invitrogen, Carlsbad, CA) and visualized on microscope.

Enzyme-linked immunosorbent assay (ELISA) for detection of human lambda immunoglobulin

Cells were infected with MV-Lambda and then treated with Y27632 in a similar manner as described above. At specified time point 100 μL of media was removed for analysis. Quantitative ELISA for human lambda immunoglobulin was performed using an ELISA kit (Bethyl Laboratories, Montgomery, TX) following the manufacturer's protocol.

To assess the impact of inhibition of fusion fusion-inhibitory peptide (FIP) (Z-D-Phe-L-Phe-Gly-OH [Bachem, Torrance, Ca]) (20 μg/ml) was added to select wells after incubation with

the MV to inhibit F-protein function and block syncytia formation. ELISA to detect human light chain lambda was performed as described above.

SDS-PAGE immunoblot

Supernatants and cell lysates were prepared from MDA-MB-231 cells infected with MV-GFP (MOI of 0.01). Uninfected cells were used as controls. Proteins were resolved on 12.5% polyacrylamide gels using Criterion electrophoresis system (Bio-Rad, Hercules, CA). For immunoblotting, SDS-PAGE fractionated proteins were blotted on PVDF membranes (Bio-Rad) using semi-dry transfer system (Bio-Rad, Hercules, CA). 5–10% non-fat dry milk (Bio-Rad, Hercules, CA) in PBS/T was used for blocking. Membranes were incubated with supernatant dilutions of Anti-N mouse antibody developed in our laboratory (publication pending) overnight at 4°C. Rabbit mouse specific polyvalent immunoglobulin (G, A, M) HRPO conjugate (diluted 1:2000 in 5% dry milk in PBS/T) was used as secondary antibody (Pierce, Rockford, IL). Specific protein bands were visualized using chemiluminescent reagent (Pierce, Rockford, IL).

In vivo experiments

All animal studies were approved by the Mayo Foundation Institutional Animal Care and Use Committee. Mice were maintained in the animal facilities of Mayo Clinic, Rochester MN.

Subcutaneous MDA-MB-231 tumor model

Xenografts derived from the MDA-MB-231 cell line were established into the right flanks of 6–8-week-old female BALB/c nude mice by subcutaneous injection of 5×10^6 cells suspended in 0.1 ml phosphate-buffered saline and 0.1 ml of BD Matrigel basement membrane matrix (BD Biosciences, Bedford, MA). The mice were examined daily for tumor growth. Tumor volume was measured with calipers twice weekly and calculated by the formula: volume = $[(\text{smallest diameter})^2 \times (\text{largest diameter})]/2$. Once all tumors were > 500 mm^3 mice were randomly divided into 2 groups (n=3). All tumors received injection with 1.5×10^6 $TCID_{50}$ MV-Lambda. Subsequently, the mice were treated either with 100 mL of PBS or Y27632 dissolved in PBS at 10 mg/kg through intra-abdominal injection twice daily. On day 5 mice were euthanized and blood was collected. Serum was analyzed with quantitative ELISA for lambda detection as described above.

Statistical analysis

Statistical comparisons were carried out using the Student *t* test. The data obtained are expressed as mean ± standard deviation (SD). *P* values of <0.05 were considered statistically significant.

Acknowledgments

Supported in part by NIH grants P50CA136393, P50108961, R01 CA136547, R01 CA154348.

Bibliography

1. Yanagi Y. The cellular receptor for measles virus--elusive no more. Rev Med Virol. 2001; 11:149–156. [PubMed: 11376478]
2. Frenzke M, Sawatsky B, Wong XX, et al. Nectin-4-dependent measles virus spread to the cynomolgus monkey tracheal epithelium: role of infected immune cells infiltrating the lamina propria. J Virol. 2013; 87:2526–2534. [PubMed: 23255790]
3. Muhlebach MD, Mateo M, Sinn PL, et al. Adherens junction protein nectin-4 is the epithelial receptor for measles virus. Nature. 2011; 480:530–533. [PubMed: 22048310]

4. Iorio RM, Melanson VR, Mahon PJ. Glycoprotein interactions in paramyxovirus fusion. Future Virol. 2009; 4:335–351. [PubMed: 20161127]
5. Navaratnarajah CK, Oezguen N, Rupp L, et al. The heads of the measles virus attachment protein move to transmit the fusion-triggering signal. Nat Struct Mol Biol. 2011; 18:128–134. [PubMed: 21217701]
6. Wild TF, Malvoisin E, Buckland R. Measles virus: both the haemagglutinin and fusion glycoproteins are required for fusion. J Gen Virol. 1991; 72(Pt 2):439–442. [PubMed: 1993882]
7. Smith EC, Popa A, Chang A, Masante C, Dutch RE. Viral entry mechanisms: the increasing diversity of paramyxovirus entry. Febs J. 2009; 276:7217–7227. [PubMed: 19878307]
8. Kallewaard NL, Bowen AL, Crowe JE Jr. Cooperativity of actin and microtubule elements during replication of respiratory syncytial virus. Virology. 2005; 331:73–81. [PubMed: 15582654]
9. Bedows E, Rao KM, Welsh MJ. Fate of microfilaments in vero cells infected with measles virus and herpes simplex virus type 1. Mol Cell Biol. 1983; 3:712–719. [PubMed: 6343843]
10. Stallcup KC, Raine CS, Fields BN. Cytochalasin B inhibits the maturation of measles virus. Virology. 1983; 124:59–74. [PubMed: 6681685]
11. Berghall H, Wallen C, Hyypia T, Vainionpaa R. Role of cytoskeleton components in measles virus replication. Arch Virol. 2004; 149:891–901. [PubMed: 15098105]
12. Duprex WP, McQuaid S, Rima BK. Measles virus-induced disruption of the glial-fibrillary-acidic protein cytoskeleton in an astrocytoma cell line (U-251). J Virol. 2000; 74:3874–3880. [PubMed: 10729162]
13. Wurth MA, Schowalter RM, Smith EC, Moncman CL, Dutch RE, McCann RO. The actin cytoskeleton inhibits pore expansion during PIV5 fusion protein-promoted cell-cell fusion. Virology. 2010; 404:117–126. [PubMed: 20537366]
14. Zohn IM, Campbell SL, Khosravi-Far R, Rossman KL, Der CJ. Rho family proteins and Ras transformation: the RHOad less traveled gets congested. Oncogene. 1998; 17:1415–1438. [PubMed: 9779988]
15. Mukai M, Togawa A, Imamura F, et al. Sustained tyrosine-phosphorylation of FAK through Rho-dependent adhesion to fibronectin is essential for cancer cell migration. Anticancer Res. 2002; 22:3175–3184. [PubMed: 12530062]
16. Itoh K, Yoshioka K, Akedo H, Uehata M, Ishizaki T, Narumiya S. An essential part for Rho-associated kinase in the transcellular invasion of tumor cells. Nat Med. 1999; 5:221–225. [PubMed: 9930872]
17. Yamana N, Arakawa Y, Nishino T, et al. The Rho-mDia1 pathway regulates cell polarity and focal adhesion turnover in migrating cells through mobilizing Apc and c-Src. Mol Cell Biol. 2006; 26:6844–6858. [PubMed: 16943426]
18. Yoshioka K, Matsumura F, Akedo H, Itoh K. Small GTP-binding protein Rho stimulates the actomyosin system, leading to invasion of tumor cells. J Biol Chem. 1998; 273:5146–5154. [PubMed: 9478968]
19. Imamura F, Mukai M, Ayaki M, et al. Involvement of small GTPases Rho and Rac in the invasion of rat ascites hepatoma cells. Clin Exp Metastasis. 1999; 17:141–148. [PubMed: 10411106]
20. Wyckoff JB, Pinner SE, Gschmeissner S, Condeelis JS, Sahai E. ROCK- and myosin-dependent matrix deformation enables protease-independent tumor-cell invasion in vivo. Curr Biol. 2006; 16:1515–1523. [PubMed: 16890527]
21. Chrzanowska-Wodnicka M, Burridge K. Rho-stimulated contractility drives the formation of stress fibers and focal adhesions. J Cell Biol. 1996; 133:1403–1415. [PubMed: 8682874]
22. Worthylake RA, Burridge K. RhoA and ROCK promote migration by limiting membrane protrusions. J Biol Chem. 2003; 278:13578–13584. [PubMed: 12574166]
23. Ashida N, Arai H, Yamasaki M, Kita T. Distinct signaling pathways for MCP-1-dependent integrin activation and chemotaxis. J Biol Chem. 2001; 276:16555–16560. [PubMed: 11278464]
24. Qiu RG, Chen J, McCormick F, Symons M. A role for Rho in Ras transformation. Proc Natl Acad Sci U S A. 1995; 92:11781–11785. [PubMed: 8524848]
25. Suwa H, Ohshio G, Imamura T, et al. Overexpression of the rhoC gene correlates with progression of ductal adenocarcinoma of the pancreas. Br J Cancer. 1998; 77:147–152. [PubMed: 9459160]

26. Clark EA, Golub TR, Lander ES, Hynes RO. Genomic analysis of metastasis reveals an essential role for RhoC. Nature. 2000; 406:532–535. [PubMed: 10952316]
27. Allen C, Opyrchal M, Aderca I, et al. Oncolytic measles virus strains have significant antitumor activity against glioma stem cells. Gene Ther. 2012
28. Opyrchal M, Allen C, Iankov I, et al. Effective radiovirotherapy for malignant gliomas by using oncolytic measles virus strains encoding the sodium iodide symporter (MV-NIS). Hum Gene Ther. 2012; 23:419–427. [PubMed: 22185260]
29. Allen C, Paraskevakou G, Iankov I, et al. Interleukin-13 displaying retargeted oncolytic measles virus strains have significant activity against gliomas with improved specificity. Mol Ther. 2008; 16:1556–1564. [PubMed: 18665158]
30. Allen C, Paraskevakou G, Liu C, et al. Oncolytic measles virus strains in the treatment of gliomas. Expert Opin Biol Ther. 2008; 8:213–220. [PubMed: 18194077]
31. Liu C, Sarkaria JN, Petell CA, et al. Combination of measles virus virotherapy and radiation therapy has synergistic activity in the treatment of glioblastoma multiforme. Clin Cancer Res. 2007; 13:7155–7165. [PubMed: 18056196]
32. Paraskevakou G, Allen C, Nakamura T, et al. Epidermal growth factor receptor (EGFR)-retargeted measles virus strains effectively target EGFR- or EGFRvIII expressing gliomas. Mol Ther. 2007; 15:677–686. [PubMed: 17299404]
33. Allen C, Vongpunsawad S, Nakamura T, et al. Retargeted oncolytic measles strains entering via the EGFRvIII receptor maintain significant antitumor activity against gliomas with increased tumor specificity. Cancer Res. 2006; 66:11840–11850. [PubMed: 17178881]
34. McDonald CJ, Erlichman C, Ingle JN, et al. A measles virus vaccine strain derivative as a novel oncolytic agent against breast cancer. Breast Cancer Res Treat. 2006; 99:177–184. [PubMed: 16642271]
35. Iankov ID, Msaouel P, Allen C, et al. Demonstration of anti-tumor activity of oncolytic measles virus strains in a malignant pleural effusion breast cancer model. Breast Cancer Res Treat. 2010; 122:745–754. [PubMed: 19894113]
36. Dingli D, Peng KW, Harvey ME, et al. Image-guided radiovirotherapy for multiple myeloma using a recombinant measles virus expressing the thyroidal sodium iodide symporter. Blood. 2004; 103:1641–1646. [PubMed: 14604966]
37. Studebaker AW, Kreofsky CR, Pierson CR, Russell SJ, Galanis E, Raffel C. Treatment of medulloblastoma with a modified measles virus. Neuro Oncol. 2010; 12:1034–1042. [PubMed: 20494960]
38. Studebaker AW, Hutzen B, Pierson CR, Russell SJ, Galanis E, Raffel C. Oncolytic measles virus prolongs survival in a murine model of cerebral spinal fluid-disseminated medulloblastoma. Neuro Oncol. 2012; 14:459–470. [PubMed: 22307474]
39. Msaouel P, Iankov ID, Allen C, et al. Noninvasive imaging and radiovirotherapy of prostate cancer using an oncolytic measles virus expressing the sodium iodide symporter. Mol Ther. 2009; 17:2041–2048. [PubMed: 19773744]
40. Msaouel P, Iankov ID, Allen C, et al. Engineered measles virus as a novel oncolytic therapy against prostate cancer. Prostate. 2009; 69:82–91. [PubMed: 18973133]
41. Blechacz B, Splinter PL, Greiner S, et al. Engineered measles virus as a novel oncolytic viral therapy system for hepatocellular carcinoma. Hepatology. 2006; 44:1465–1477. [PubMed: 17133484]
42. Peng KW, TenEyck CJ, Galanis E, Kalli KR, Hartmann LC, Russell SJ. Intraperitoneal therapy of ovarian cancer using an engineered measles virus. Cancer Res. 2002; 62:4656–4662. [PubMed: 12183422]
43. Galanis E, Hartmann LC, Cliby WA, et al. Phase I trial of intraperitoneal administration of an oncolytic measles virus strain engineered to express carcinoembryonic antigen for recurrent ovarian cancer. Cancer Res. 2010; 70:875–882. [PubMed: 20103634]
44. Ulloa L, Serra R, Asenjo A, Villanueva N. Interactions between cellular actin and human respiratory syncytial virus (HRSV). Virus Res. 1998; 53:13–25. [PubMed: 9617766]
45. Giuffre RM, Tovell DR, Kay CM, Tyrrell DL. Evidence for an interaction between the membrane protein of a paramyxovirus and actin. J Virol. 1982; 42:963–968. [PubMed: 6285006]

46. Burke E, Mahoney NM, Almo SC, Barik S. Profilin is required for optimal actin-dependent transcription of respiratory syncytial virus genome RNA. J Virol. 2000; 74:669–675. [PubMed: 10623728]
47. Wang JL, Zhang JL, Chen W, et al. Roles of small GTPase Rac1 in the regulation of actin cytoskeleton during dengue virus infection. PLoS Negl Trop Dis. 2010; 4
48. Ishizaki T, Uehata M, Tamechika I, et al. Pharmacological properties of Y-27632, a specific inhibitor of rho-associated kinases. Mol Pharmacol. 2000; 57:976–983. [PubMed: 10779382]
49. Nishimura Y, Itoh K, Yoshioka K, Tokuda K, Himeno M. Overexpression of ROCK in human breast cancer cells: evidence that ROCK activity mediates intracellular membrane traffic of lysosomes. Pathol Oncol Res. 2003; 9:83–95. [PubMed: 12858212]
50. de Toledo M, Anguille C, Roger L, Roux P, Gadea G. Cooperative anti-invasive effect of Cdc42/Rac1 activation and ROCK inhibition in SW620 colorectal cancer cells with elevated blebbing activity. PLoS One. 2012; 7:e48344. [PubMed: 23144867]
51. Lawler K, Foran E, O'Sullivan G, Long A, Kenny D. Mobility and invasiveness of metastatic esophageal cancer are potentiated by shear stress in a ROCK- and Ras-dependent manner. Am J Physiol Cell Physiol. 2006; 291:C668–C677. [PubMed: 16641163]
52. Salhia B, Rutten F, Nakada M, et al. Inhibition of Rho-kinase affects astrocytoma morphology, motility, and invasion through activation of Rac1. Cancer Res. 2005; 65:8792–8800. [PubMed: 16204049]
53. Sahai E, Ishizaki T, Narumiya S, Treisman R. Transformation mediated by RhoA requires activity of ROCK kinases. Curr Biol. 1999; 9:136–145. [PubMed: 10021386]
54. Xu XT, Song QB, Yao Y, Ruan P, Tao ZZ. Inhibition of RhoA/ROCK signaling pathway promotes the apoptosis of gastric cancer cells. Hepatogastroenterology. 2012; 59:2523–2526. [PubMed: 22584506]
55. Forbes SA, Bindal N, Bamford S, et al. COSMIC: mining complete cancer genomes in the Catalogue of Somatic Mutations in Cancer. Nucleic Acids Res. 2011; 39:D945–D950. [PubMed: 20952405]
56. Fritz G, Just I, Kaina B. Rho GTPases are over-expressed in human tumors. Int J Cancer. 1999; 81:682–687. [PubMed: 10328216]
57. Patel RA, Forinash KD, Pireddu R, et al. RKI-1447 is a potent inhibitor of the Rho-associated ROCK kinases with anti-invasive and antitumor activities in breast cancer. Cancer Res. 2012; 72:5025–5034. [PubMed: 22846914]
58. Nakajima M, Hayashi K, Egi Y, et al. Effect of Wf-536, a novel ROCK inhibitor, against metastasis of B16 melanoma. Cancer Chemother Pharmacol. 2003; 52:319–324. [PubMed: 12783205]
59. Takamura M, Sakamoto M, Genda T, Ichida T, Asakura H, Hirohashi S. Inhibition of intrahepatic metastasis of human hepatocellular carcinoma by Rho-associated protein kinase inhibitor Y-27632. Hepatology. 2001; 33:577–581. [PubMed: 11230737]
60. Iankov ID, Hillestad ML, Dietz AB, Russell SJ, Galanis E. Converting tumor-specific markers into reporters of oncolytic virus infection. Mol Ther. 2009; 17:1395–1403. [PubMed: 19471250]
61. Duprex WP, McQuaid S, Roscic-Mrkic B, Cattaneo R, McCallister C, Rima BK. In vitro and in vivo infection of neural cells by a recombinant measles virus expressing enhanced green fluorescent protein. J Virol. 2000; 74:7972–7979. [PubMed: 10933705]
62. Duprex WP, McQuaid S, Hangartner L, Billeter MA, Rima BK. Observation of measles virus cell-to-cell spread in astrocytoma cells by using a green fluorescent protein-expressing recombinant virus. J Virol. 1999; 73:9568–9575. [PubMed: 10516065]
63. Anderson BD, Nakamura T, Russell SJ, Peng KW. High CD46 receptor density determines preferential killing of tumor cells by oncolytic measles virus. Cancer research. 2004; 64:4919–4926. [PubMed: 15256464]

A. MDA-MB-231

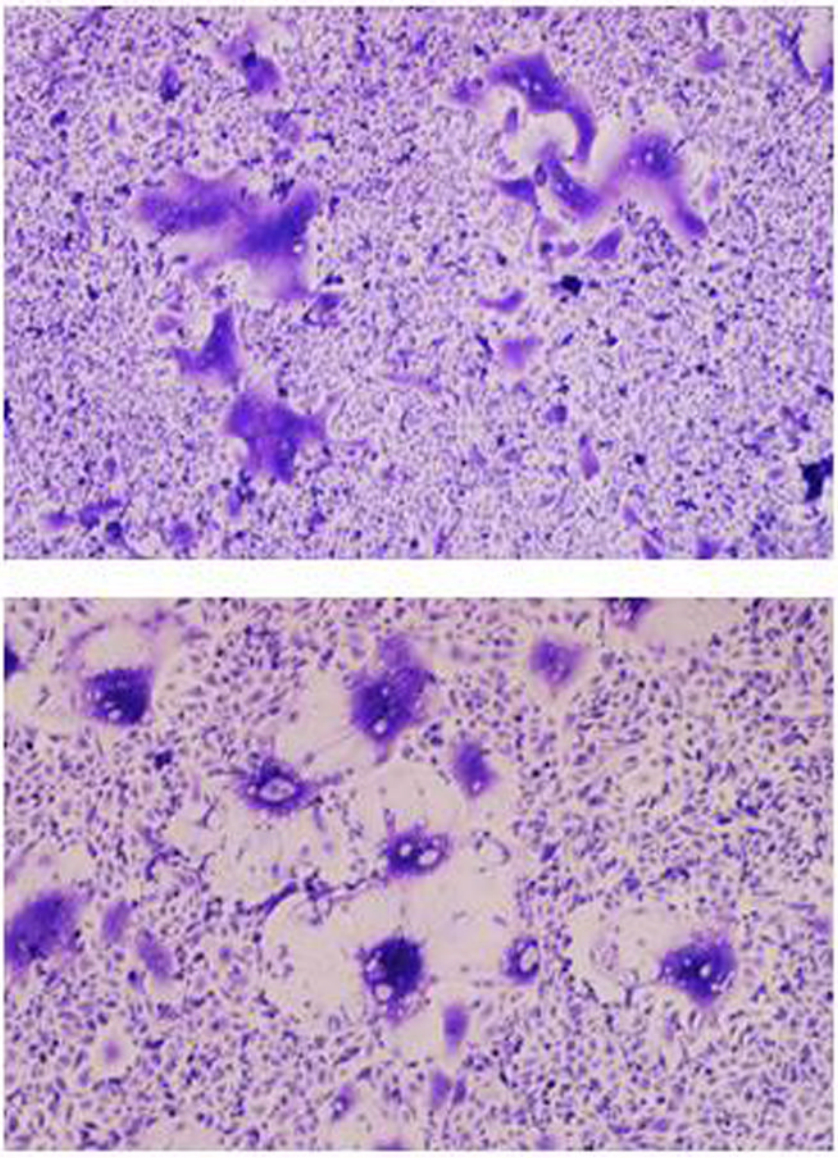

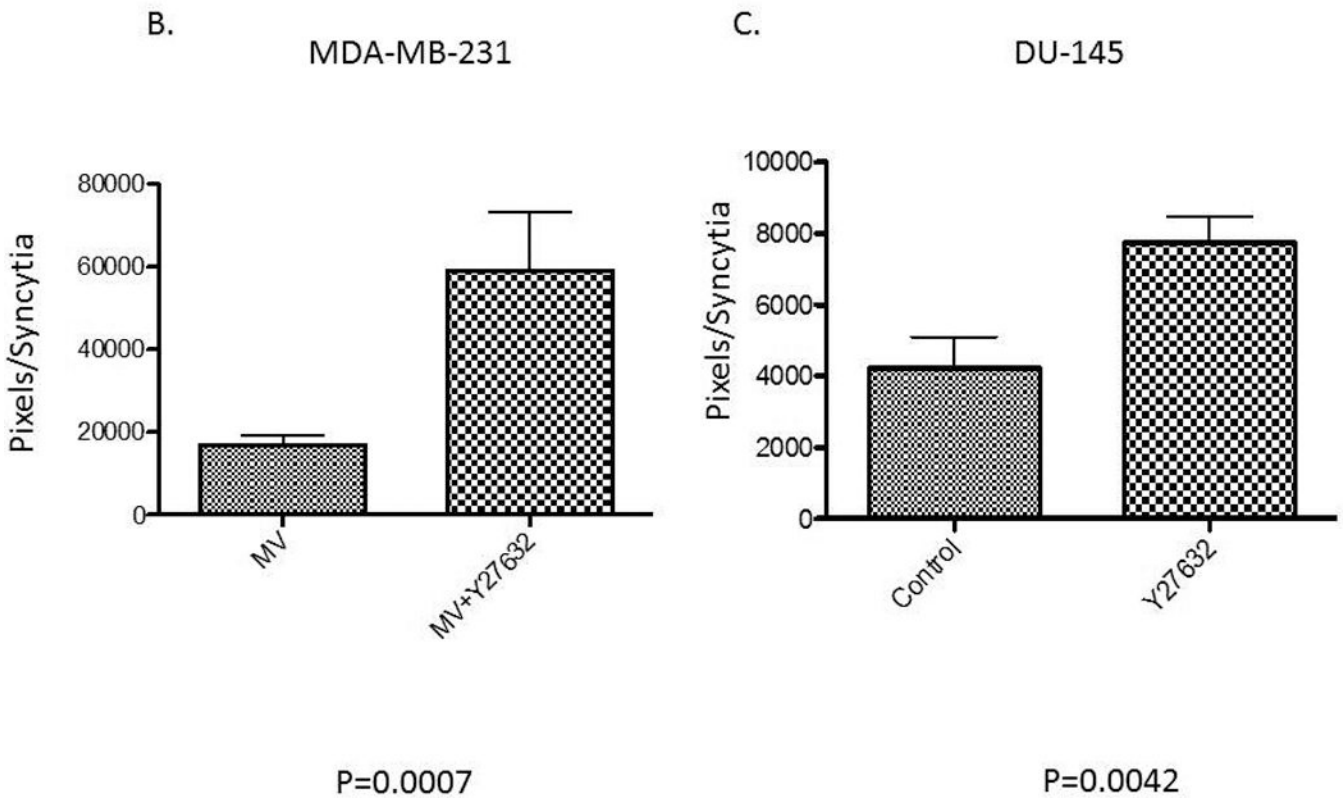

Figure 1. Treatment with Y27632 causes increased measles virus induced syncytia *in vitro*

Picture of representative syncytia in MDA-MB-231 cells (A) or DU-145 (B) cells 48–72 hours after infection with MV-GFP (MOI 0.1) alone (upper panels) or in presence of Y27632 (150 μM (A) and 100 μM (B)) (lower panels). The syncytia areas were then quantified and the average size of syncytia represented in MDA-MB-231 cells (C) and DU-145 cells (D). P values calculated when comparing syncytia in MV-GFP infected cells in absence or presence of Y27632 are shown below the graphs.

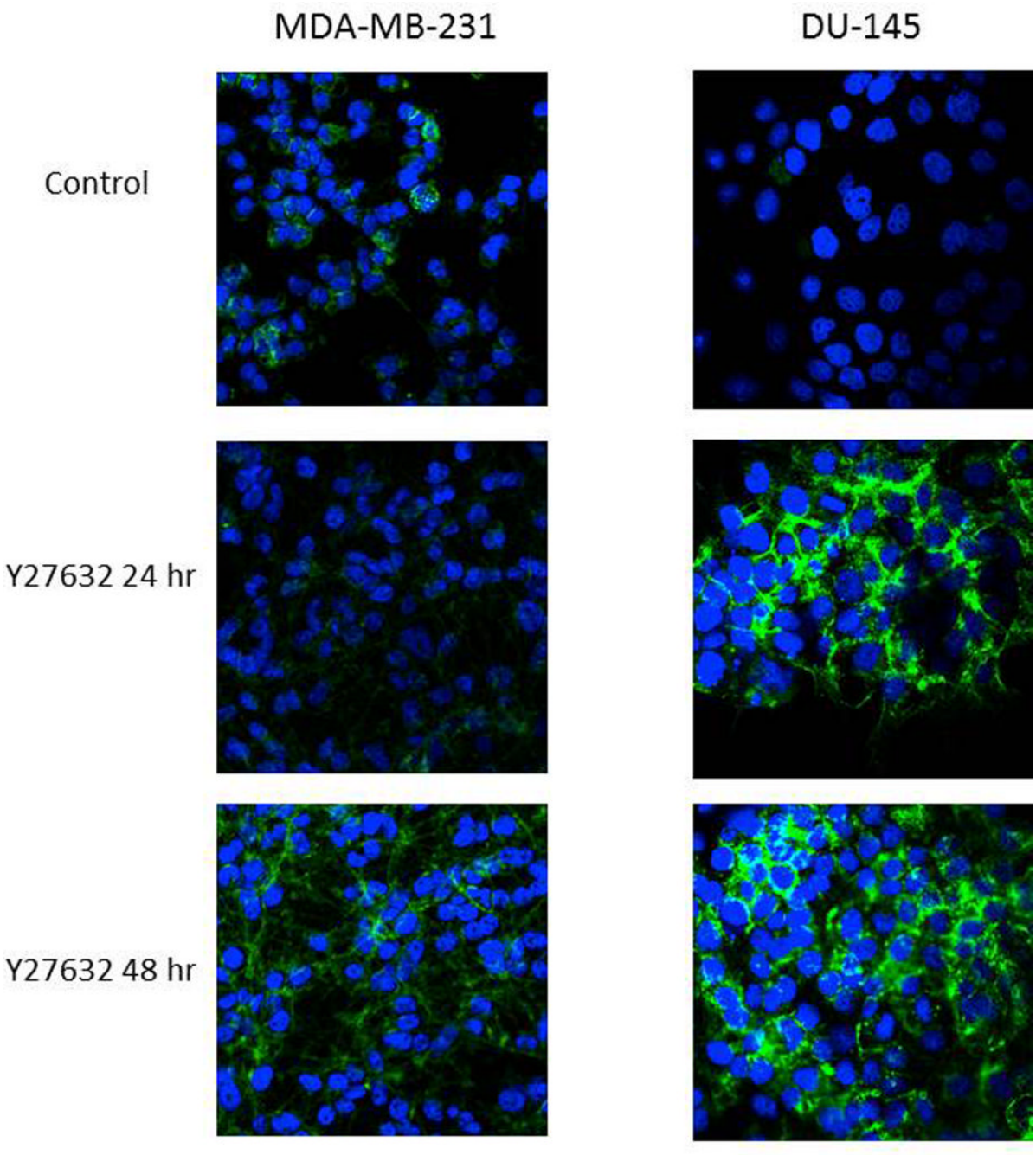

Figure 2. Treatment with Y27632 causes profound disruption of the actin cytoskeleton

MDA-MB-231 and DU-145 were incubated for 48 hours alone (control) or with Y27632 (150 μM for 24 or 48 hours with MDA-MB-231 cells or 100 μM for 24 or 48 hours with DU-145 cells). The cells were stained with conjugated phallotoxin binding to F-actin and photographed. The representative photos are displayed with DAPI staining representing nuclei.

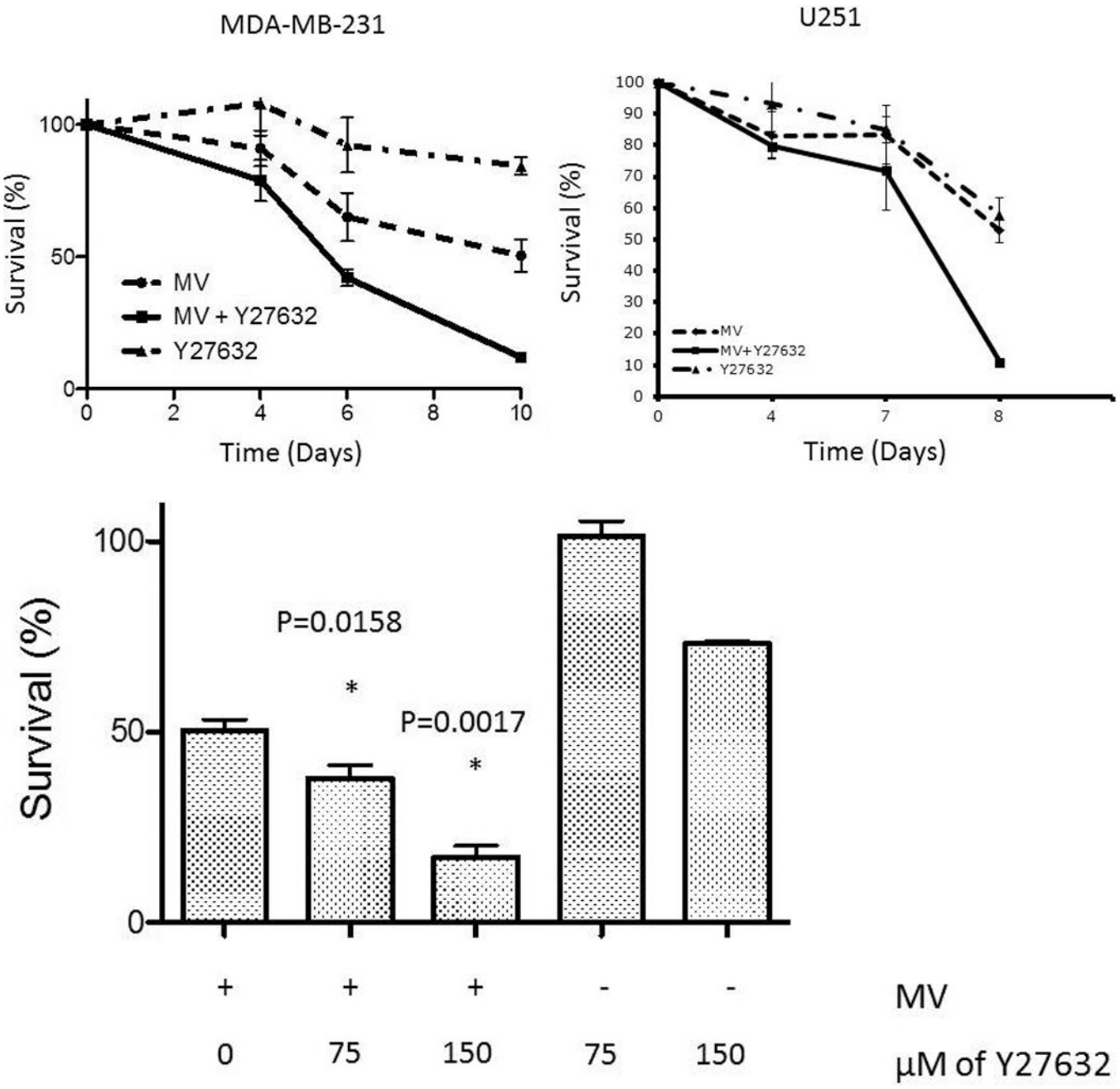

Figure 3. Treatment with Y27632 causes increased measles virus induced cytopathic effect *in vitro*

A. Cytopathic effect of MV-GFP on MDA-MB-231 and U251 at 0.01 MOI as determined by trypan blue exclusion assay alone or in combination with 150 µM or 25 µM respectively of Y27632. Y27632 alone was used as control. Combination of MV-GFP and Y27632 led to faster elimination of tumor cell monolayers when compared to either therapy alone.

B. Percent of cells surviving as determined by trypan blue exclusion assay on day 7 after incubation with MV-GFP concurrently treated with increasing concentrations of Y27632 as noted on the graph.

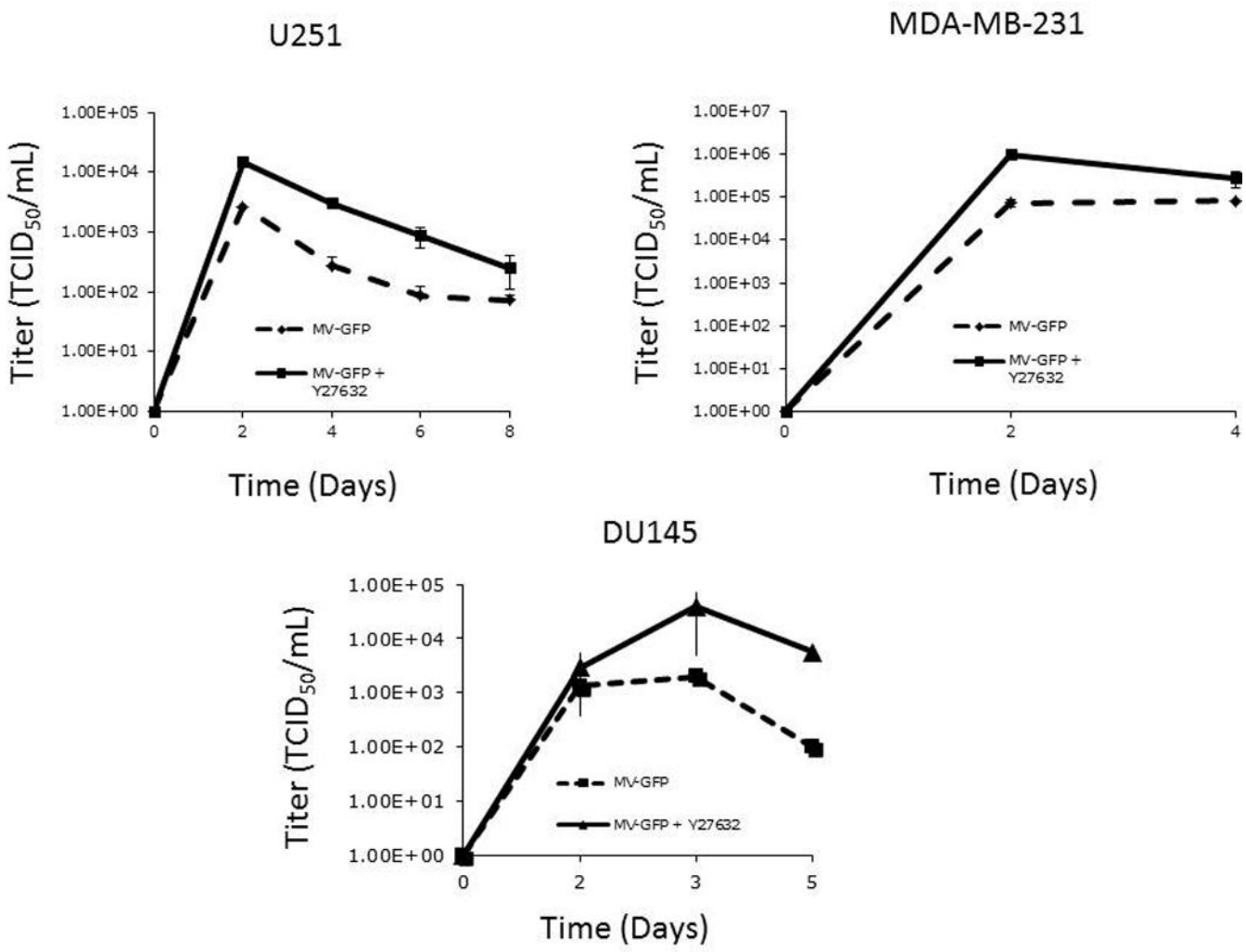

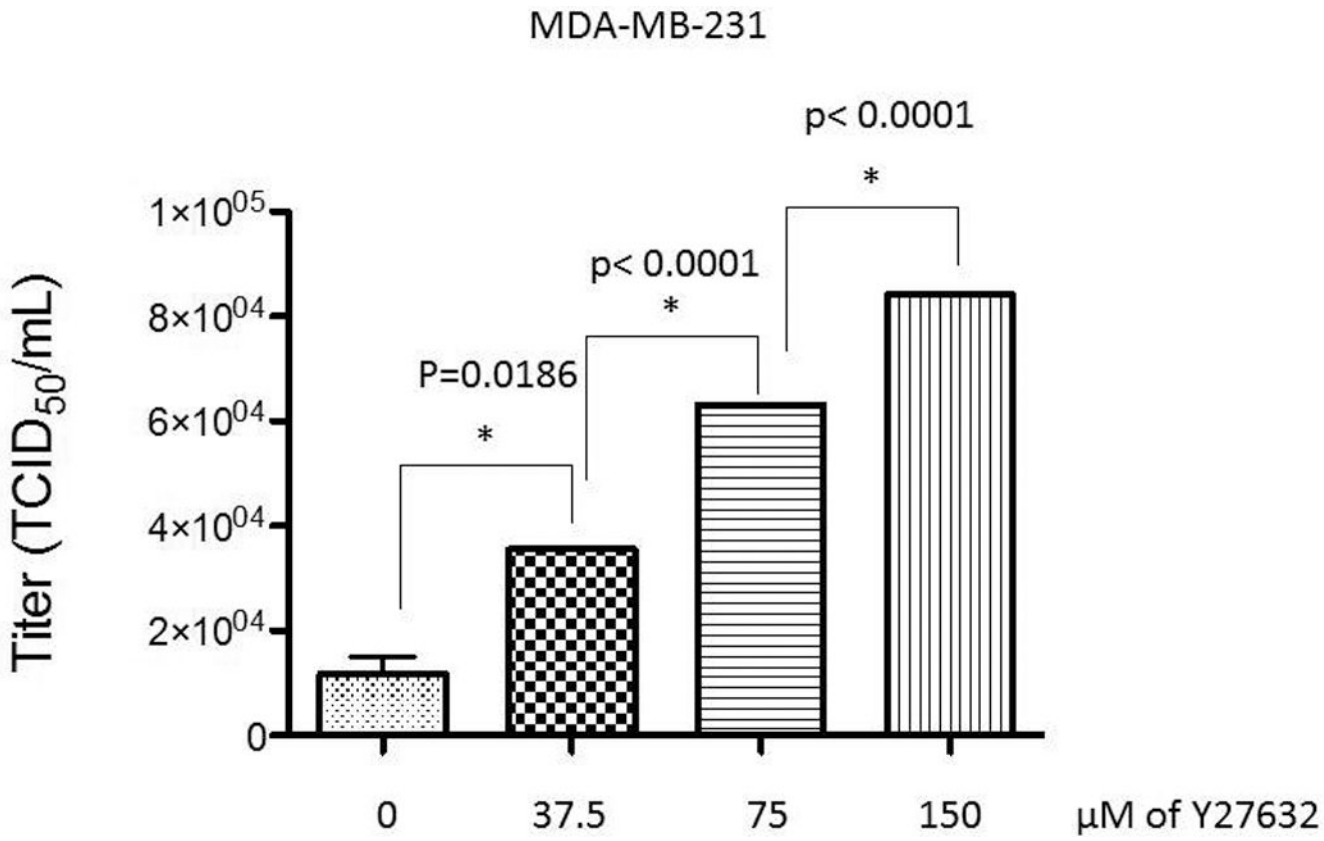

Figure 4. Treatment with Y27632 causes increased measles virus replication *in vitro*

A. One step viral growth curves demonstrate more rapid replication of MV-GFP after infection at MOI of 0.01 when cells were also treated with Y27632 in MDA-MB-231, U251 and DU145 cells.

B. The $TCID_{50}$/mL on day 2 after infection of MV-GFP at MOI of 0.01 increases in presence of increasing concentrations of Y27632. P values are noted above the graph.

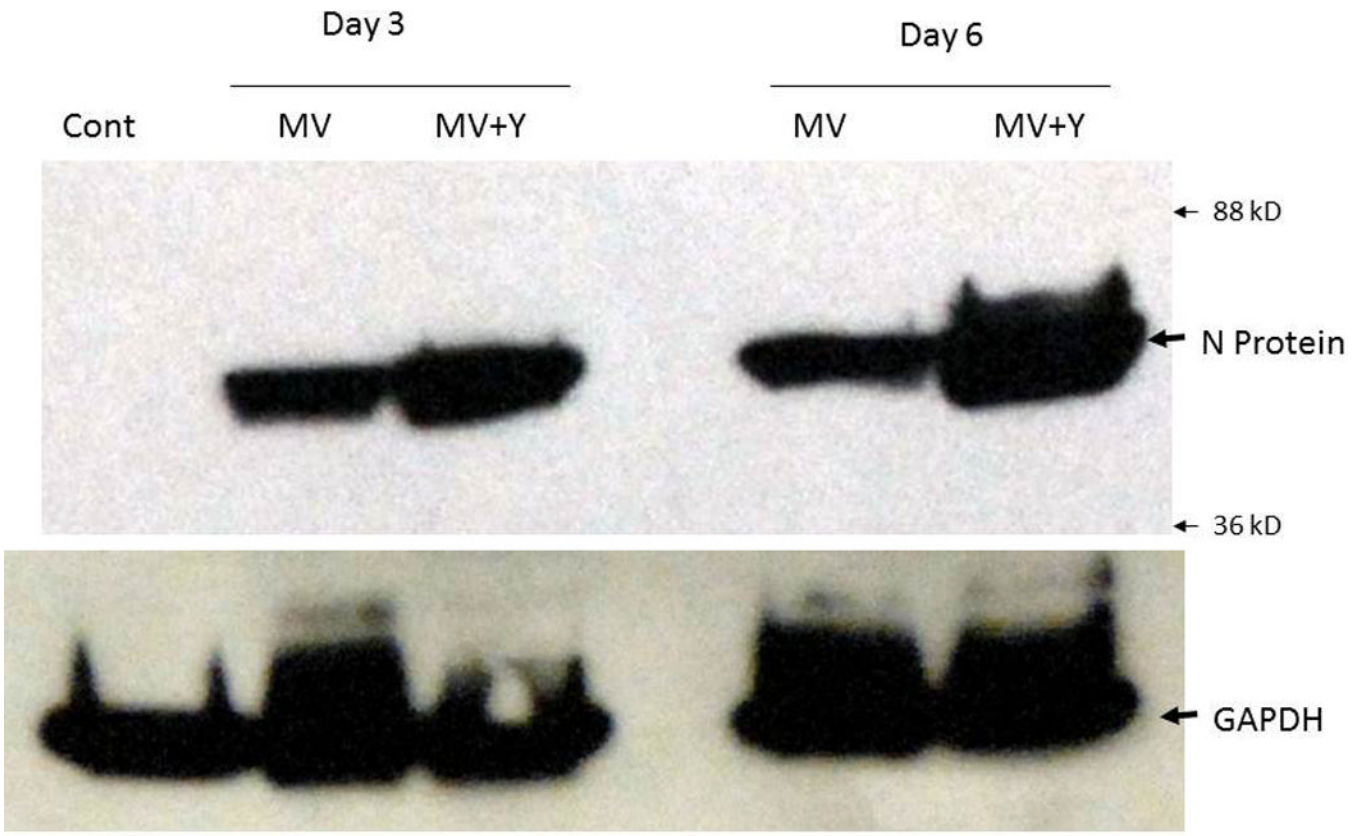

Figure 5. Treatment with Y27632 causes increased viral protein production in MV-GFP infected cells *in vitro*

MDA-MB-231 cells infected with MV-GFP (or uninfected controls) were lysed on day 3 and 6 and total protein was separated by electrophoresis. The membrane was blotted for MV nucleocapsid (N) protein showing increased levels of N protein in cells treated with 150 μM of Y27632. GAPDH was used as a loading control.

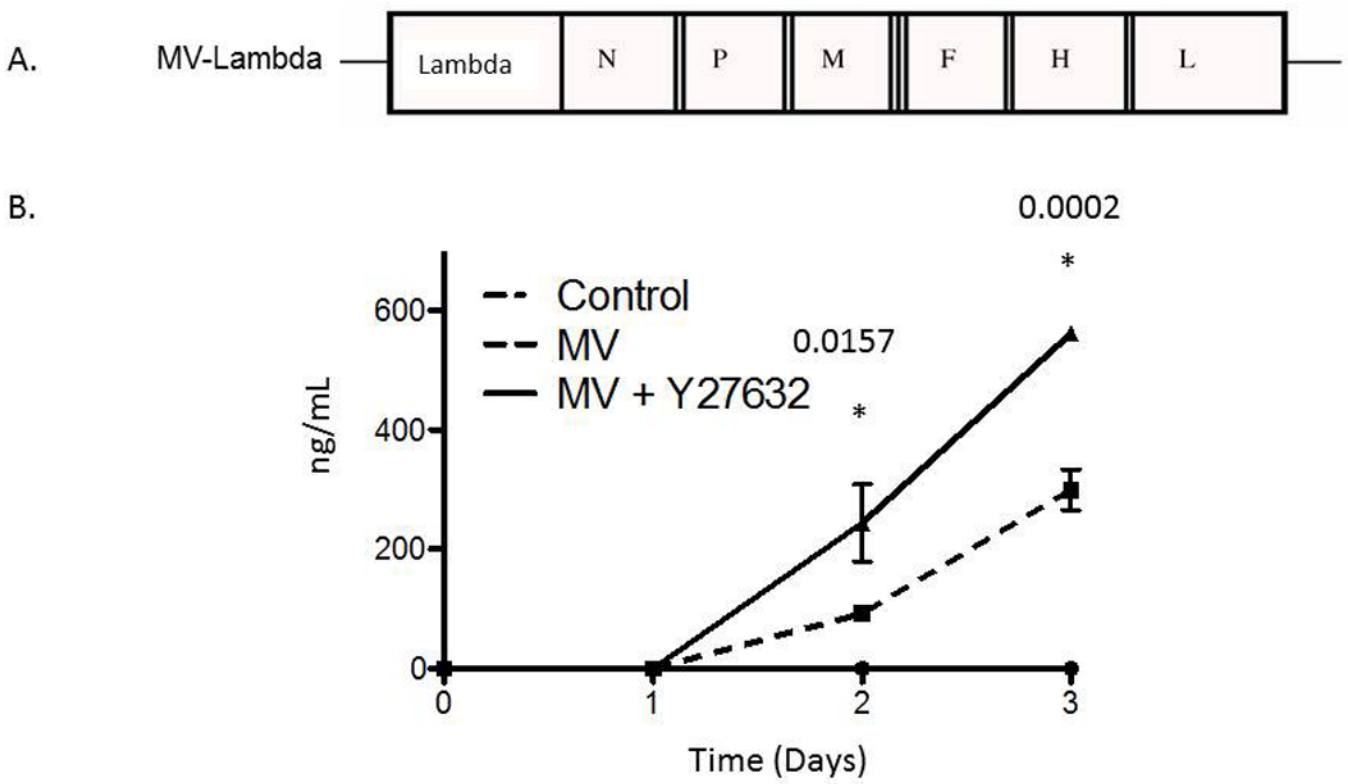

Figure 6. Treatment with Y27632 causes increased production of lambda protein *in vitro*

A. Schematic representation of MV-Edm strain, MV-Lambda. N, nucleoprotein gene; L, large protein gene; P, phosphoprotein gene; M, matrix protein gene; F, fusion protein gene; H, hemaglutinin gene; lambda, human lambda light chain gene.

B. Treatment with Y27632 causes increased production of lambda when compared to MV-Lambda infection alone. Uninfected control cells did not produce any detectable levels of human lambda.

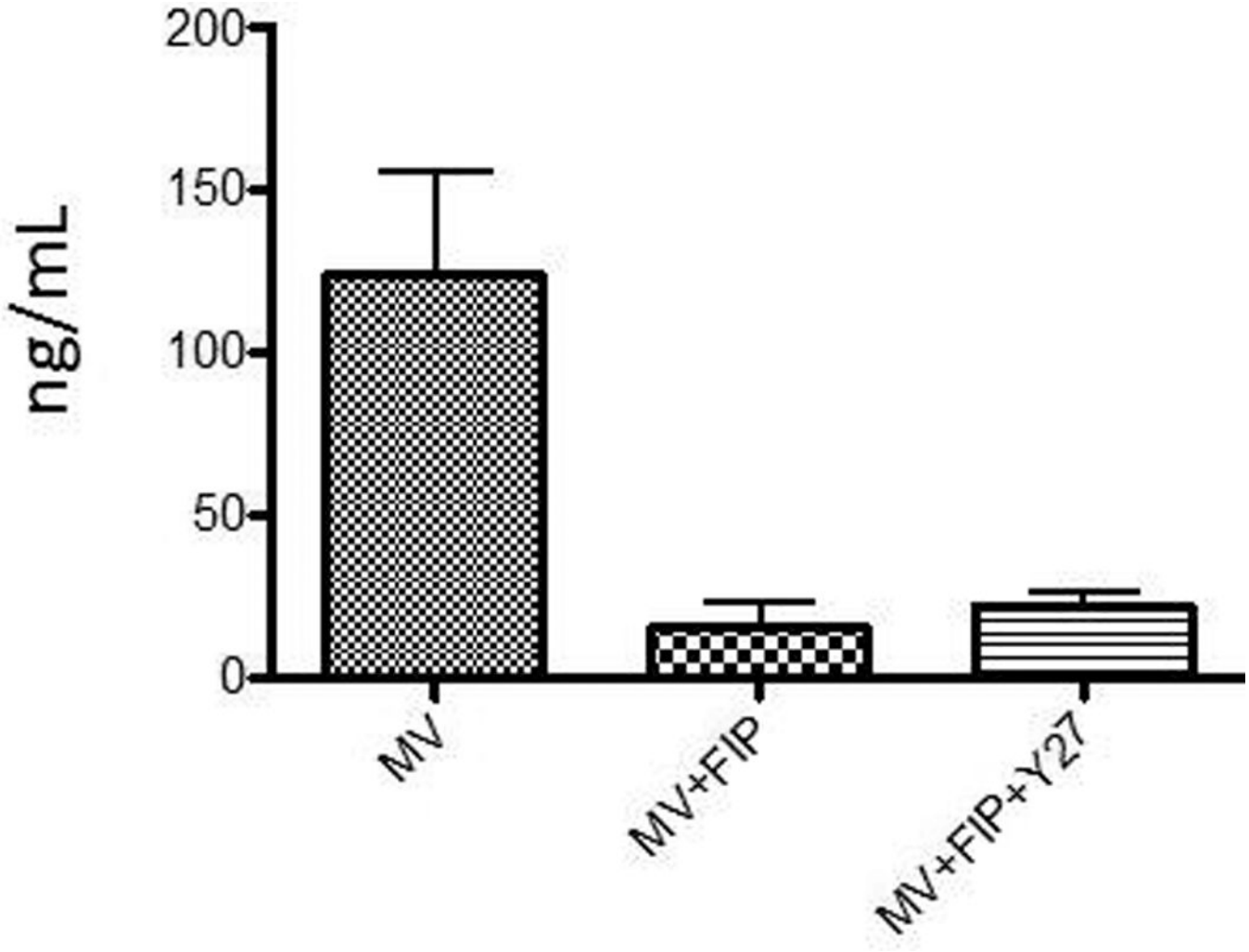

Figure 7. Syncytia necessary for the effect of Y27632 on viral replication *in vitro*

Cells grown in 6 well plates were infected with MV-Lambda at MOI of 0.01 and then were treated with FIP or vehicle alone. Additionally, cells treated with FIP were treated with 150 μM of Y27632 or vehicle alone. 48 hours after the infection the growth media was analyzed by ELISA for levels of lambda light chain, levels from 3 plates were reported on the graph.

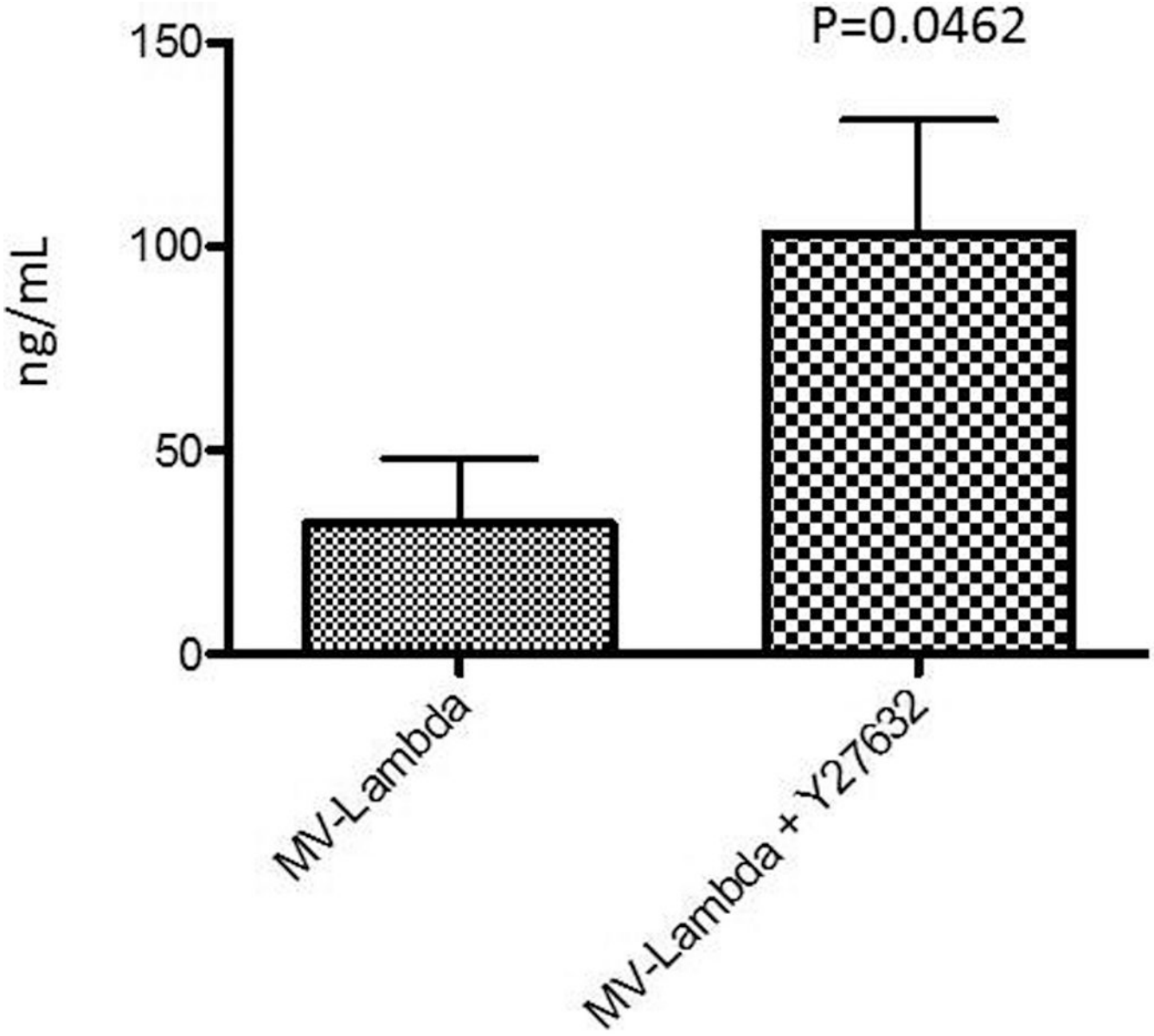

Figure 8. Treatment with Y27632 causes increased production of lambda protein *in vivo*

2 groups of BALB/c nude mice (n=3) and control group were subcutaneously implanted with $5*10^6$ MDA-MB-231 cells. After animals had flank tumors established (> 600 mm^3) they were treated with one intratumoral injection of MV-Lambda $2*10^6$ $TCID_{50}$. Treatment group received Y27632 through intraperitoneal injection twice daily at 10 mg/kg dose for a total of 10 doses. On day 5 blood was obtained from the animals and isolated serum was tested for levels of human lambda levels. Control animals did not have any detectable levels. Levels were reported in ng/mL and p value calculated is shown on the graph.